Design and Integration of an Underactuated Robotic Finger with Vision-based Tactile Sensing

by

Yuxiang Ma

Submitted to the Department of Mechanical Engineering
in partial fulfillment of the requirements for the degree of

MASTER OF SCIENCE IN MECHANICAL ENGINEERING

at the

MASSACHUSETTS INSTITUTE OF TECHNOLOGY

September 2023

Authored by: Yuxiang Ma
Department of Mechanical Engineering
August 27, 2023

Certified by: Edward H. Adelson
John and Dorothy Wilson Professor of Vision Science, Thesis Supervisor

Accepted by: Nicolas Hadjiconstantinou
Professor
Graduate Officer, Department of Mechanical Engineering

Design and Integration of an Underactuated Robotic Finger with Vision-based Tactile Sensing

by

Yuxiang Ma

Submitted to the Department of Mechanical Engineering
on August 27, 2023 in partial fulfillment of the requirements for the degree of

MASTER OF SCIENCE IN MECHANICAL ENGINEERING

ABSTRACT

Underactuated fingers are adaptable to different shapes, robust, and cost-effective for executing sturdy and versatile grasps. However, they generally have limited control or require complex planning when performing tasks that require high precision or delicate handling. Vision-based tactile sensors, like GelSight, can mitigate these control issues by adding real-time proprioception and also provide useful high-resolution tactile information, which can enhance underactuated fingers with shape and texture perception. As such, this work presents the development of a compact, underactuated linkage finger and its integration with a low-cost, simple vision-based tactile sensor, i.e. the Gelsight.

Through the process of developing the tactile, linkage fingers, we established a planar linkage mechanism simulator and a simple 2D ray-tracing optical simulator to help optimize the linkage transmission and improve tactile sensing performance. In total, the finger went through three major designs. In the initial iteration, we designed sliding joints, which were replaced in the second iteration by linkage mechanisms to make the design more compact and robust. A planar linkage simulator was used to optimize the trajectory to avoid collision and increase range of motion. In the current iteration, the finger has evolved from having two segments to having three segments, with underactuation incorporated to further reduce the number of motors. Each finger segment houses a silicone gel pad, whose tactile imprints are captured by mirrors, which are then observed by a single camera placed at the second finger segment. The camera and mirrors are positioned based on the results of a simple ray-tracing simulator, which guaranteed that each finger segment could be visible in all finger configurations.

The use of mirrors, linkage transmission and underactuation makes the mechanism compact, efficient, and less complex by reducing the number of cameras and motors needed. Moreover, the integration of vision-based sensors allows these underactuated fingers to perceive contact information and finger configuration. In conclusion, this work encapsulates the innovative design and integration of an underactuated linkage finger with vision-based tactile sensing, offering compactness, adaptability, and robustness in grasping tasks. Additionally, the integration of vision-based tactile sensors can significantly enhance the capabilities of underactuated fingers by providing them with high resolution images and proprioception information, and potentially broaden the future usage of underactuated fingers.

Thesis supervisor: Edward H. Adelson
Title: John and Dorothy Wilson Professor of Vision Science

Acknowledgments

This work is financially supported by the Toyota Research Institute.

First and foremost, I would like to thank my advisor, Edward Adelson, for all of his help and support. I would like to acknowledge Alan Zhao for his efforts in makeing early prototype designs and discussions, Sandra Liu for her help in experiments and fabrication, and Megha Tippur for her help in designing PCBs. I would also thank Branden Romero, Maria Ramos Gonzalez, and Alan Papalia for their suggestions and feedback. Finally, I want to acknowledge my parents and my friends for their support during my study and research.

Contents

List of Figures

List of Tables

Chapter 1

Introduction

Various robotic hands has been designed to complete grasping and manipulation tasks. Researchers have employed different mechanisms, e.g. tendons[1], [2], linkages[3], compliant structures[4]–[6], vacuum[7], hydraulics [6] and pneumatic [8], to satisfy the requirements demanded by different applications, such as surgeries, prosthesis, manufacturing, agriculture etc.

Over all kinds of grippers, parallel-jaw grippers has become one of the most popular choices in both industry and academia because of its simplicity and low cost. As the name suggests, parallel-jaw grippers feature two opposing jaws that move in parallel to each other to grasp objects. This design allows for a straightforward and reliable grasping on objects with various shapes and sizes, but grasping objects with complex shapes or unusual sizes might be a issue due to its lack of adaptation. Parallel-jaw grippers has been particularly popular in some basic manipulation tasks where high precision and force regulation are not required, e.g. pick-and-place operations and bin picking. However, its performance in dexterous tasks, e.g. fine grasping, tool using and in-hand manipulation, is greatly limited with only one degree of freedom.

Despite the fact that parallel-jaw grippers have been the most popular choice in industry and academia, the field still looks forward to the development of anthropomorphic hands

(or dexterous hands) that replicates human hand functions [3]. Until now, there are already several commercialized humanoid hands available, e.g. the Shadow Dexterous Hand [9], the Allegro Hand [10] and other hands. Besides, many researchers have been exploring different possible designs of anthropomorphic hands [1]–[3], [8], [11]. Typically, dexterous hands have more than ten degrees of freedom and requires the same or less actuators. Arranging large number of joints and actuators in a robot hand is quite challenging, especially when compact and low-cost designs are preferred. In addition, large number of DOFs also leads to the difficulty of motion planning and control [12], [13].

Nowadays, building a versatile robotic hand remains challenging, because an over-complicated design with many joints and actuators would be impractical to build and control. Many researcher has been trying to find a compromise between dexterity and simplicity. The most straight forward approach is reducing the dofs by coupling the motion of several joints, but this often leads to a decrease in adaptability and dexterity. Another approach is using a small number of actuators without reducing the number of joints. One implementation is using clutches to control the engagement between several joints and one actuator [14]. But in this case, joints have to be actuated in a sequence, which again limits the hand performance in dexterous tasks. Another more popular implementation consists in underactuated mechanisms, which utilize passive elements or joint limits to reduce the amount of actuators.

Underactuation has become an emerging topic in the field of robotics. Because of its light weight, ease of control and low energy consumption, It has been applied to almost every robotic domain which requires multiple DOF robot design and control, including walking mechanisms, robot arms, robot wrists and robot hands. When it comes to robot hands, the designs that involves underactuated mechanisms can be divided into finger designs and whole hand designs. There are more works about underactuated fingers because it is relatively easier to design and manufacture. Underactuated finger design is focused on actuation and transmission of one single finger as well as its workspace and adaptability, while the whole hand design that involves underactuated mechanisms puts more emphasis on multiple-finger

synergies[15]. The latter approach can reduce the amount of actuators to two or three, but usually a big number of pulleys and tendons have to be embedded in the hand, which leads to complicated manufacturing and assembly. Furthermore, designing multi-finger synergies is also a non-trivial task. This work focuses on underactuated finger designs. Aside from reducing complexity and cost, underactuated mechanism allows the finger to conform to various object, commonly known as adaptation. The adaptive behavior further expands the application of underactuated fingers. For example, in grasping tasks, stable grasping of a wide array of unfamiliar objects can be easily achieved with underactuated fingers, while complicated control policies and motion planning algorithms have to be employed for fully actuated hands or fingers.

Despite their advantages, underactuated fingers also present challenges that must be overcome to fully unleash their potential. Many underactuated fingers exhibit reduced precision and accuracy due to its lack of actuation. Besides uncertainty in finger motion, less actuators also brought the problem of limited control. For tasks that requires precision and fine control, developing effective control strategies for underactuated fingers can be complex, and it may require advanced machine learning techniques or sophisticated control frameworks. By addressing the limitations and optimizing their mechanical design and control strategies, underactuated fingers hold promise for a future where robots can handle complex and dynamic real-world scenarios with dexterity, sensitivity, and grace.

Sensory feedback, such as proprioception and tactile sensing, can potentially augment the functionality of underactuated fingers. Proprioception, referred to the perception of internal states of a robot, can provide information about the finger movement and further help to improve control precision. But unlike fully actuated fingers, in which accurate joint angles can be easily acquired from motor encoders, obtaining the joint angles of underactuated fingers is a non-trivial task because the configuration of underactuated fingers can not be determined with only encoder data. Thus, proprioception of underactuated fingers requires other sensing modalities to provide extra information. One example is that some tactile

sensors are capable of perceiving the internal states of robotic fingers, such as vision-based tactile sensors [16]. Meanwhile, tactile sensing can provide contact information about the touched objects, including contact geometry, contact force or wrench, sliding and vibration. These information can both benefit the feedback control of underacted fingers and enhance their performance in manipulation tasks.

This work developed an underactuated finger integrated with vision-based tactile sensing, which provides tactile images and proprioception information. In order to obtain a compact and high-efficient design, we reduced the amount of actuators by adopting an underactuated linkage mechanism that is optimized with a linkage simulation algorithm. For the integration of tactile sensing, this work employed a kind of vison-based tactile sensor, i.e. Gelsight. It has the advantage of high resolution and low-cost. To keep the design compact even after integrated with tactile sensing, this work combined Gelsight with mirrors, which are placed at specific positions to make sure the camera has a good view of all sensing patches. The final design has three phalanges, two dofs and only one actuator. All three phalanges are embedded with tactile sensing patches. A computer vision algorithm is also established to stably obtain undistorted tactile images. Meanwhile, proprioception is achieved with the same algorithm, which evaluates joint angles of the underactuated finger with high accuracy. The integration of vision-based tactile sensors can significantly enhance the capabilities of underactuated fingers by providing them with high resolution images and proprioception information, and potentially broaden the future usage of underactuated fingers.

Chapter 2

Related Work

2.1 Underactuated Fingers

Underactuated robot fingers represent a significant advancement in the realm of robotics, offering unique advantages that can revolutionize human-robot interactions and enable robots to perform various tasks with greater adaptability and efficiency. These fingers are designed with fewer degrees of freedom than the number of joints they could potentially control, resulting in a mechanically simpler and lighter system. Thanks to the prosperity of underactuated robotics in recent years, various underactuated mechanisms have been employed to build low-cost, adaptive and robust robotic fingers.

Underactuated fingers can be divided into two types, rigid fingers and soft (or compliant) fingers. Soft fingers or compliant fingers are commonly considered to have infinite degrees of freedom, which makes them extremely adaptive and flexible. These fingers are usually actuated by pneumatic actuators or by tendon-driven mechanisms. Pneumatic actuators are less popular in rigid fingers, and this work focuses on actuation of rigid fingers. For rigid fingers, popular underactuated mechanisms includes tendon-driven mechanisms, differential mechanisms and underactuated linkage mechanisms. In tendon-driven underactuated fingers, tendons and flexors connect the actuators to the finger joints. The total number of

tendons and flexors is fewer than the finger's DOF, leading to coupled motion between joints. Tendon-drive mechanisms are bio-inspired and high-efficient, but it introduces backlash and hysteresis to the finger due to slippage and wear and is sensitive to the tension of tendons. These issues make them hard to manufacture and less favorable for high-precision tasks. Differential mechanisms use a combination of gears, springs, or linkages to distribute the actuation force across multiple joints. By adjusting the actuation input, the finger can achieve various grasping configurations, effectively reducing the number of actuators required. Differential mechanisms are compact and high-efficient, but designing a differential mechanism is complicated. Besides, differential mechanisms has high requirements on manufacturing tolerance, and bad tolerance influences its precision and accuracy. Underactuated linkage mechanisms combine the principles of underactuation with the use of linkage systems, resulting in designs that can achieve complex motions with fewer actuators than degrees of freedom. Compact and high-efficient designs can be easily achieved, and it has lower requirement on manufacturing tolerance comparing with differential mechanisms. However, linkage mechanisms could lead to limited ranges of motion and unnatural trajectory if not designed properly.

This work designed underactuated linkage mechanisms to keep the whole finger compact, low-cost and easy to manufacture. The author established a 2D linkage mechanism simulator to optimize motion trajectory and expand ranges of motion.

2.2 Underactuated fingers integrated with tactile sensing

Underactuated robot fingers have fewer degrees of freedom compared with fully actuated ones, making them suitable for lightweight and simplified designs. However, underactuated robot fingers often face challenges in terms of limited control and sensing capabilities compared to fully actuated ones. Researchers have been combining tactile sensors with underactuated fingers to overcome these difficulties.

Tactile sensors consists of a wide range of devices that employs different principles, including capacitive sensors, piezoelectric sensors, piezoresistive sensors, and vision-based tactile sensors. Among those sensors, the former three are more conventional and popular, and they are based on changes in electric properties, i.e. capacitance, resistance and voltage. Until now, most research that involves both underactuated finger and tactile sensing has employed these electrical sensors, because of their simplicity and ease of integration. Spider et al. implemented tactile object identification and feature extraction techniques on a two-phalanx finger embedded with eight barometric pressure sensors [17]. Although with sparse tactile information, the gripper was able to classify objects and estimate stiffness, size and pose of the grasped object. Similarly, Yoon et al. proposed a tendon-driven robotic finger design that incorporated stretchable tactile sensors, which are made from ecoflex and liquid metal and utilize piezoresistive effect of liquid metal. Using the sensor information, the gripper was able to grasp a inflated balloon and maintain a desired contact pressure with force feedback control. Lu et al. combined underactuated linkage mechanism with arrays of biomimetic tactile sensors, which measures both normal and shear force [18]. The gripper was able to grasp various everyday objects and achieve in-hand manipulation including translation and rotation with closed-loop control. By applying machine learning methods, Puhlmann et al. proposed an approach for estimating the pose of in-hand objects combining tactile sensing data and visual frames of reference [19] With a fuzzy controller, the gripper was able to achieve and sustain stable grasping conditions autonomously while forces were applied to in-hand objects to expose the system to different object configurations, which shows tactile sensing can help grippers to make more stable and sturdy grasps.

Up to now, all research that involves both underactuated fingers and tactile sensing uses pressure or force sensors. These sensors have high frequency response (around 100 Hz) and are amenable to be integrated in robots, and some papers have shown promising result of augmenting underactuated fingers with tactile sensors. However, these force or pressure sensors typically have low sensing resolution and are usually made of stiff materials, which is

not favorable in scenarios that involve interaction with human or delicate objects. Not only Vision-based tactile sensors have high sensing resolution, but also they are more compatible with various computer vision algorithms and the prospering learning-based robotic control paradigms. Vision-based tactile sensing is suitable to be integrated with these underactuated fingers, helping the fingers achieve more dexterous and intuitive grasping and enhance manipulation capabilities. Although various compact and simple tactile sensors have been invented [20]–[23], it is still a non-trivial work to integrate vision-based tactile sensors with multi-phalanx fingers, including underactuated fingers. To speed up designing and sensorization, we developed a optical simulator to optimize the embedding design of vion-based tactile sensors.

2.3 Vision-based Tactile Sensing

Vision-based tactile sensors use cameras or depth sensors to obtain tactile images, which are compatible with various computer vision algorithms. By virtue of the very developed camera technology, high resolution tactile images can be easily obtained in vision-based tactile sensors. After applying computer vision algorithms, the tactile images can be interpreted as varied tactile information, e.g. contact geometry, contact force or wrench, sliding, etc [22]–[26]. With the ability to provide rich and detailed contact information, these sensors have the potential to enhance robot capabilities in dexterous manipulation, object recognition, and human-robot interactions. Meanwhile, vision-based tactile sensors used soft rubber to make contact with objects or environment, which offers firmer and safer grips and further greatly broadens the application range of robot grippers. The GelSight sensor captures images of a gel surface with an miniaturized camera, which provide high-resolution tactile information when the sensor comes into contact with an object. The using of mirror and illumination design of the integrated tactile sensing in Section 3.2 is inspired by the structure of the GelSight Wedge sensor [22].

Currently, there are many different vision-based sensors for tactile sensing developed for parallel-jaw grippers and fingertips of multi-phalanx fingers [20]–[22], [25], [27], [28]. Those designs have simple structures and provide rich tactile information. However, these designs are not enough to fully sensorise a multi-phalanx finger or a humanoid finger. There are a few attempts to integrate tactile sensing with multi-phalanx fingers. Wilson *et al.* proposed a design that embeds one tactile sensor for each phalanx of a two-phalanx finger[29]. Similarly, Liu *et al.* designed a two-phalanx soft finger with an embedded camera that captures tactile images for every phalanx. This approach works well for hands with small number of phalanges, but it would require a lot of cameras, cables and video streaming communication for a humanoid hand that has four or five fingers, which makes the robotic system complicated and cumbersome. Inspired by using mirror reflection to make a compact sensor in Gelsight Wedge [22], this work sensorised a three-phalanx finger with only one camera and two mirrors. By optimizing the positions of mirrors, the camera can obtain a full view of all sensing surfaces at all possible finger configurations. With a small sacrifice in sensing resolution, the amount of hardware needed for tactile sensing is greatly reduced. Meanwhile, the camera perspective changes as the finger moves, from which the specific finger configuration, i.e. proprioception, can extracted.

Chapter 3

Design and Fabrication

This chapter details the design and fabrication of an underactuated humanoid finger with embedded tactile sensing. We proposed several important functional requirements in Table 3.1. In order to build a compact but versatile robotic finger, we limit the electric hardware used for each finger to be one motor and one camera. Our design efforts are mainly devoted to designing high efficient torque transmission and embedding tactile sensing.

Table 3.1: Functional Requirements

Design requirements	Category	Description	Value
Number of phalanges	Geometry	-	3
DOF	Geometry	-	2
Number of motor	Hardware	-	1
Number of camera	Hardware	-	1
Tactile Sensing	Performance	All sensing segments must be visible	-
Linkage mechanism	Transmission	Transmission angles > 40 °	-
Range of motion	Transmission	Each joint	0-90 °

As shown in Fig. 3.1, the finger consists of three phalanges, two joints, one actuator and one camera. The three-phalanx structure is designed to mimic distal phalanx, intermediate phalanx, and proximal phalanx of human fingers. The dimensions of these phalanges are determined with respect to measurements of an average human index finger from an anthropometric study [30]. The lengths of distal, intermediate and proximal phalanges are

32mm, 23mm, and 35 mm. All three phalanges have a consistent width of 34 mm including sensing pads and transmission linkages, while the three sensing pads have a width of 24 mm. Linkage mechanisms are situated at both sides of the finger, which efficiently transmit actuation torque, as shown in Fig. 3.1 (a) and (b). An exploded view is shown in Fig. 3.6. The section view in Fig. 3.1 exhibits the hollow internal structure of the phalanges, which offers a clear light path to the embedded vision-based tactile sensing. With mirrors installed on distal and proximal phalanges, the camera mounted on the intermediate phalanx is able to capture images of all three sensing pads during finger movement. The arrangement of mirrors and the camera is adjusted in an optical reflection simulator to guarantee that all sensing pads can be visible to the camera during finger movement.

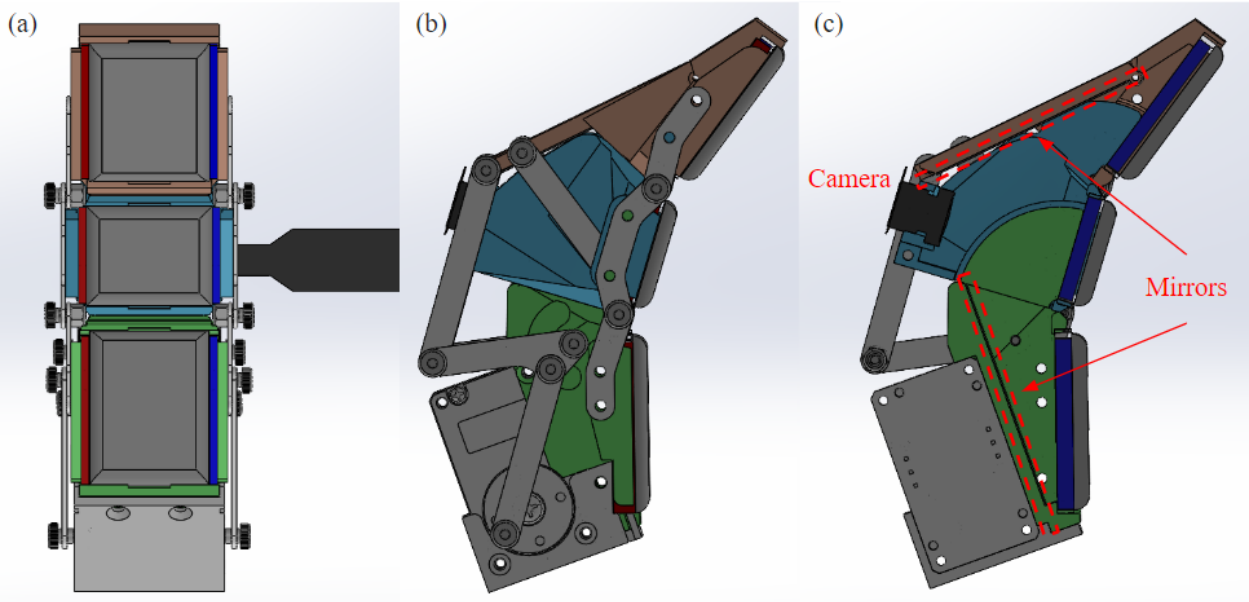

Figure 3.1: Assembled view of the proposed finger: (a) Front view; (b) Side view; (c) Section view. Phalanges are rendered in dim red, blue and green, which represent distal phalanx, intermediate phalanx, and proximal phalanx.

The proposed finger experienced several iterations, during which we developed simulation tools to guide the design process and accelerate the optimization process. The finger design consists of two main parts, linkage mechanism design and tactile sensing integration design, for which a linkage mechanism simulation tool and an optical reflection tool were separately

developed. As a consequence, fast prototypes were built, and we succeeded in creating a compact and low-cost deign as well as a simple manufacturing process.

3.1 Linkage Mechanism Design

The proposed finger employed a 2D linkage mechanism to transmit torques with high efficiency. A 2D linkage simulator was developed in Python, based on the Mechanism Python package [31]. The package is capable of implementing a kinematic analysis with the knowledge of the degrees of freedom for the vectors that make up the mechanism. With the aid of numerical solving and iteration, the position, velocity, and acceleration of these vectors and points can be acquired.

3.1.1 2D Linkage Mechanism Simulator

The developed linkage simulator analyzes the motion of linkage systems utilizing vector loops. Using the four-bar linkage in Fig. 3.2 as an example, with lengths of all four bars known, the system has only one degree of freedom. To solve the configuration of the linkage, the angles of $\overrightarrow{AB}$ and $\overrightarrow{BC}$ should be determined with the angle of $\overrightarrow{OA}$ as input. The bars should satisfy the following loop constraint:

$$\overrightarrow{OA} + \overrightarrow{AB} + \overrightarrow{BC} + \overrightarrow{CO} = \overrightarrow{0} \tag{3.1}$$

The loop constraint can be decomposed into two independent equations, e.g. along x axis and y axis.

$$L_{OA}\cos(\theta_1) + L_{AB}\cos(\theta_2) + L_{BC}\cos(\theta_3) - L_{OC} = 0 \tag{3.2}$$

$$L_{OA}\sin(\theta_1) + L_{AB}\sin(\theta_2) + L_{BC}\sin(\theta_3) = 0 \tag{3.3}$$

where $L_{OA}, L_{AB}, L_{BC}, L_{0C}$ are lengths of the corresponding links, definition of $\theta_1, \theta_2, \theta_3, \theta_4$ are angles of them, which is also shown in Fig. 3.2.

Therefore, the two unknown angles of $\overrightarrow{AB}$ and $\overrightarrow{BC}$ can be solved for each input $\overrightarrow{OA}$ angle.

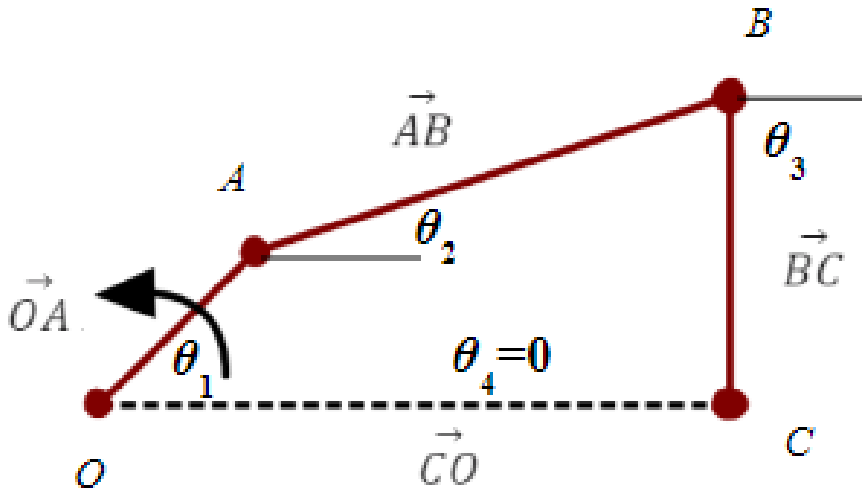

Figure 3.2: A four-bar linkage mechanism. Dashed line $\overrightarrow{CO}$ is a fixed bar; $\overrightarrow{OA}$ is an actuation bar; $\overrightarrow{AB}$ and $\overrightarrow{BC}$ are passive bars

The above simple example shows the principle of linkage mechanism simulation based on vector loops. With more nodes, bars and loops, more sophisticated mechanisms can be defined and solved.

3.1.2 Optimized Linkage Mechanism

Fig. 3.3 exhibits the linkage structure of the proposed underactuated finger. Linkages and structures affiliated to different phalanges are shown in their corresponding color, (i.e. red for distal phalanx, blue for intermediate phalanx, and green for proximal phalanx). The actual linkage mechanism consists of two parts, a six-bar linkage represented by the solid line loop $A-B-C-D-E-F-A$ and an extra constraint bar GG'. With Kutzbach's equation [32], the number of dofs should be $3(L-1)-2J-H$, where L is the number of links, $J$is the number of binary joints or lower pairs and H is the number of higher pairs. In this

case, the mechanism has seven links and eight revolute joints, which belongs to lower pairs. Therefore, the linkage has two degrees of freedom. There are many ways to choose system state variables. To make sense of the state variables, we use the angle between link OA and AB and the angle between link AB and BC, which separately correspond to proximal interphalangeal joint and distal interphalangeal joint. Link EF will be linked to a motor through a four-bar parallel motion linkage to provide actuation and transmit parallel motion. To make the mechanism underactuated, a spring is attached between link BC and link CD, as shown in Fig. 3.3.

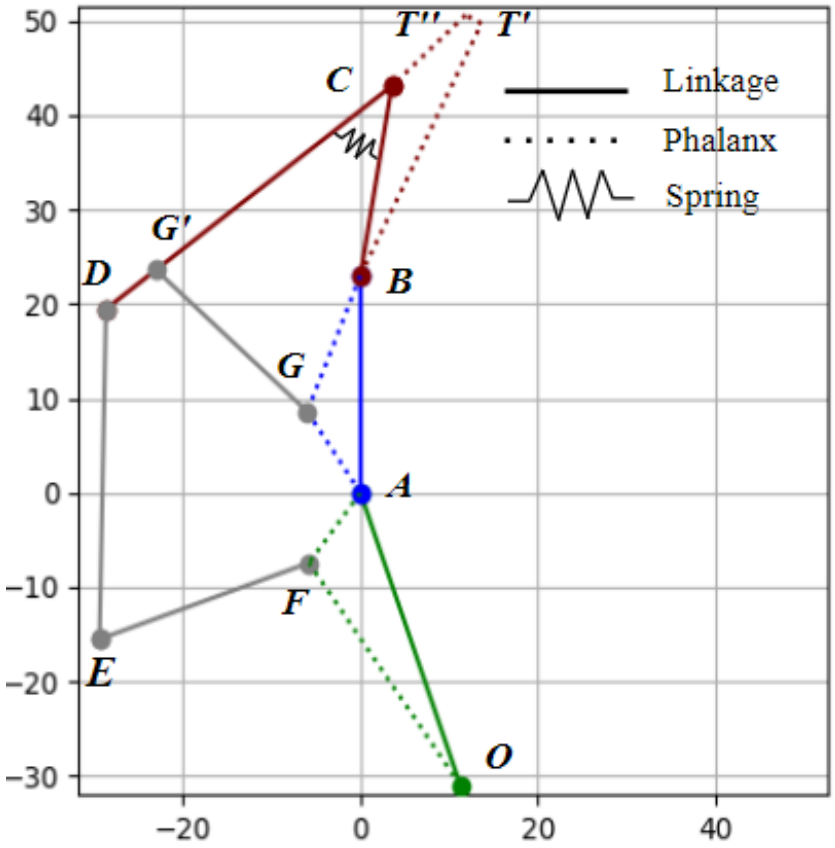

Figure 3.3: Linkage model of the underactuated finger. Solid lines stand for the actual linkage loops, while dashed lines only represent the shape and size of phalanges. The red, blue and green lines represent distal, intermediate, and proximal phalanges, and the gray lines are extra constraint bars to complement the linkage loops.

The simulator only deals with static motion analysis, so the dynamic underactuation

effect introduced by the spring can not be simulated. Because of underactuation, the finger has two motion modalities, which correspond to uncompressed spring and compressed spring. With the first input as the angle (orientation) of bar EF, the two cases can be simulated by introducing the angle between BC and CD as a secondary input. When the spring is uncompressed, the secondary input angle stays constant; when the spring is compressed, the secondary input angle becomes active.

With the above finger mechanism simulator, motion trajectories can be simulated and optimized. The optimizing constraints are two-fold. First, two finger joints should be able to rotate for 90 degrees to satisfy the functional requirement of motion range, while making the motion range of actuation bar lower than 150 degrees to avoid singular configuration. Second, there should be enough space in side each phalanx to make sure that tactile sensors will fit in them. The simulated trajectories are shown in Fig. 3.4. There are two motion modalities of the finger. The first one is when only the proximal interphalangeal joint rotates, which corresponds to the case of pinch grasping where contacts only happen to distal phalanges. The second case is that both proximal and distal interphalangeal joints are active, which corresponds to the case of adaptive grasping where contacts happen to phalanges consecutively. Pinch grasping mode can deal with smaller and delicate objects with regular shapes and operates with higher accuracy and precision, while adaptive grasping mode is able to grip bigger objects with irregular shapes and operates with higher robustness. Together, these two motion modalities empower the finger to grasp different categories of objects.

3.2 2D Reflection Simulation

In order to implement thorough and consistent tactile sensing, we built a 2D reflection simulator, which computes light rays and thus predicts the contact area that are covered by tactile sensing. The simulator was written in Python, and a simple GUI was set up using

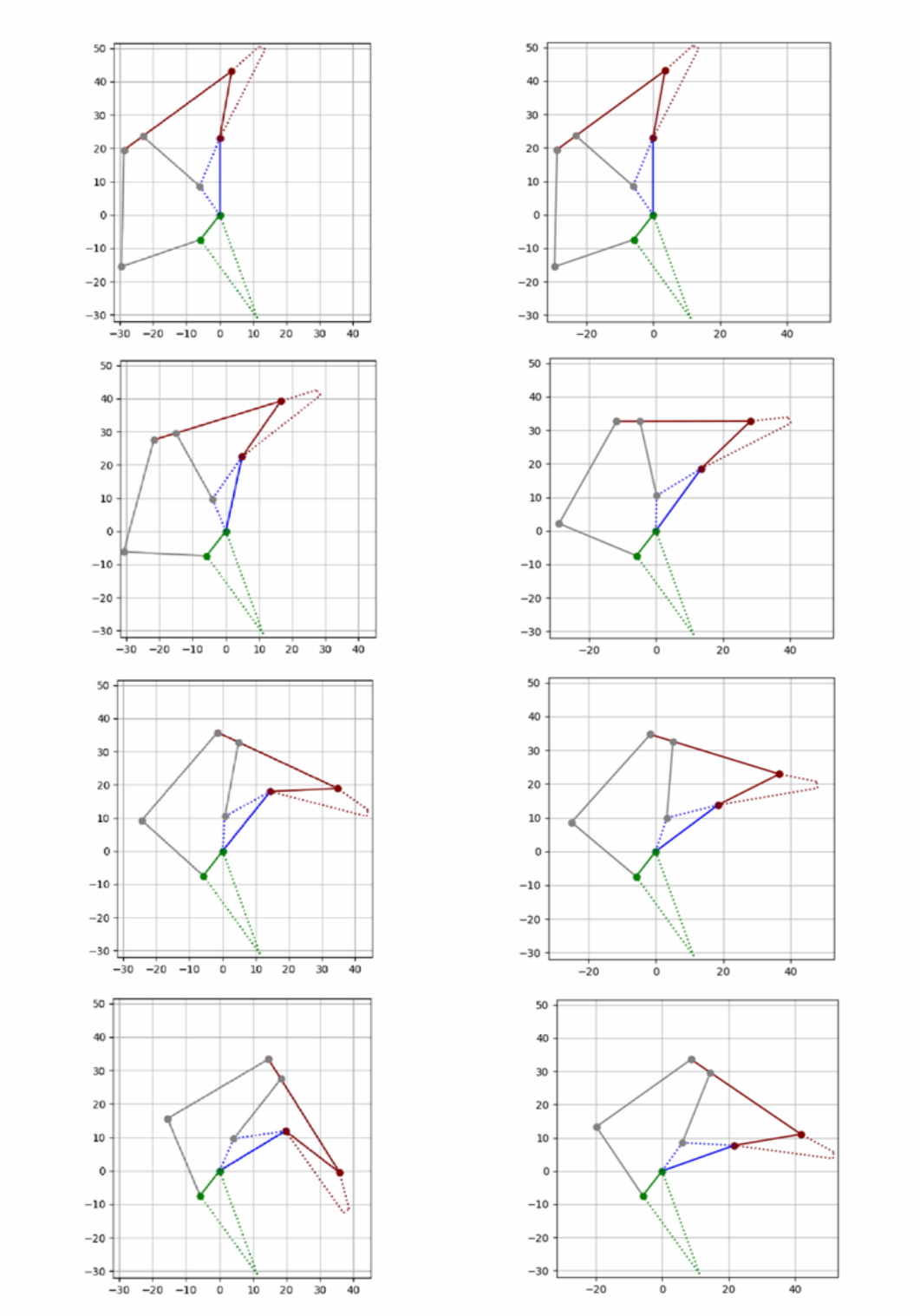

Figure 3.4: Simulated motion trajectories of the underactuated finger. From top to bottom, the finger flexes. The left and right column corresponds to the case of adaptive grasping and pinch grasping

the Matplotlib library to realize interactive optimization.

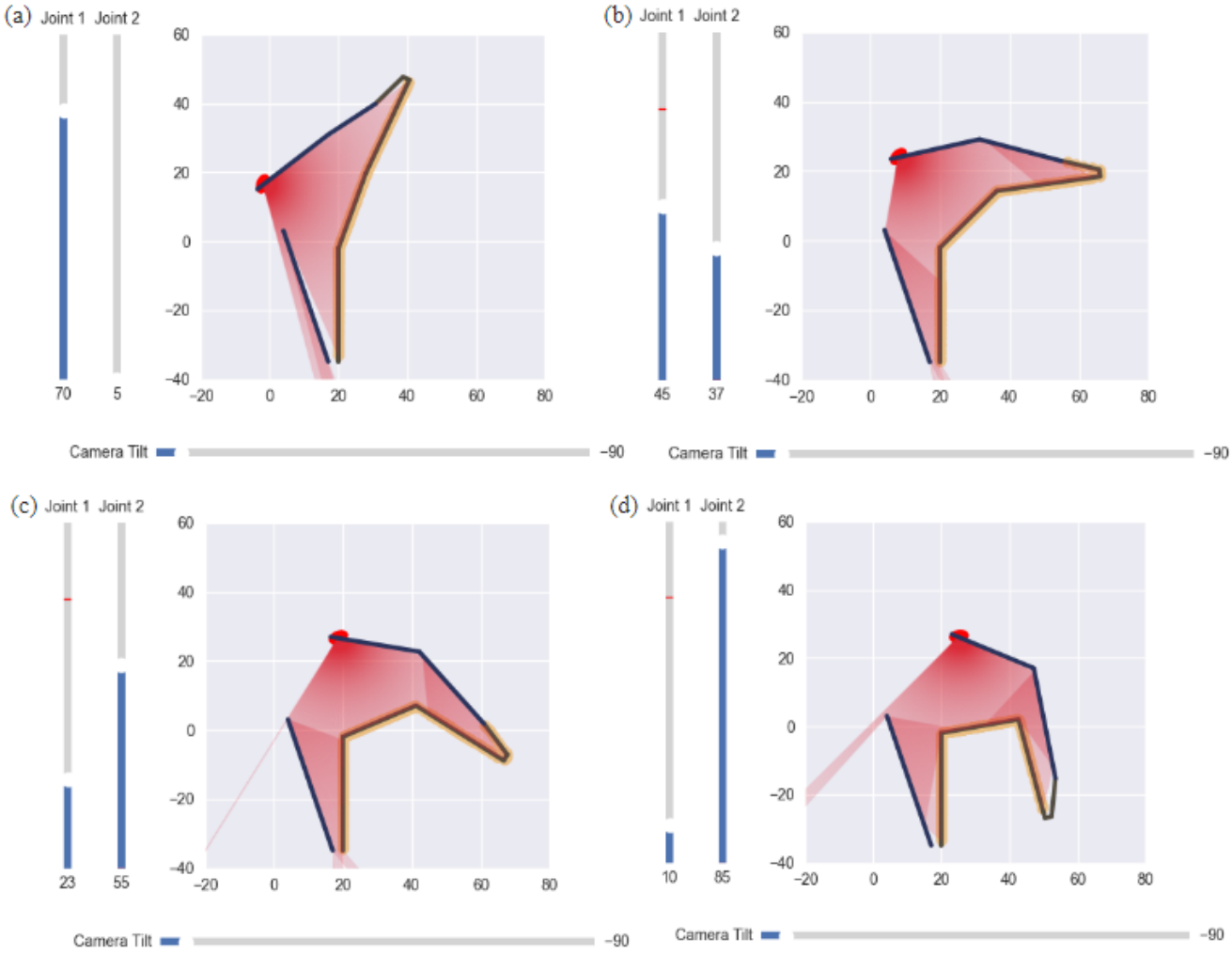

Figure 3.5: 2D reflection simulation of tactile sensing. From (a) to (d), the finger moves from its initial configuration to the fully flexed configuration. Joint 1 and 2 correspond to proximal interphalangeal joint and distal interphalangeal joint.

The reflection simulator renders the interaction between mechanical components such as mirrors and sensing pads and light rays which are highlighted with red in Fig. 3.5. The reflection is simulated based on the theory that the reflected ray and the incident ray have equal angles. In the simulator, angles of distal and interphalangeal joints can be adjusted in real time. Meanwhile, camera can be tilted in real time to obtain a better view of sensing pads. With specified finger dimensions referred to an anthropometric study [30], the positions

and lengths of mirrors and the camera are optimized in the simulator. Fig. 3.5 shows that all three finger segments are visible during finger motion, with an optimized arrangement of a camera and mirrors.

3.3 Fabrication

An exploded view of the robotic finger is displayed in Fig. 3.6. The finger fabrication can be divided into two parts, mechanical components and tactile sensing components. This section elaborates about the detailed fabrication processes of these two parts.

3.3.1 Mechanical Components

The mechanical components include phalanges, linkage bars and other accessories including shoulder screws, lock nuts and springs. The phalanges are printed with a Prusa MK3S+ printer using PLA filaments, and the linkage bars are machined from 6061 Aluminum sheets with an OMAX waterjet machine. The phalanges are carefully designed to allow the movement of links, joints, elastomer pads and the camera. Thin fins on top of intermediate and proximal phalanges are designed to block external illumination during finger movement. For the same purpose, a piece of black stretchable cloth is attached between intermediate and proximal phalanges to prevent the interference of environmental lights. With a proper tolerance, the shoulder screws and lock nuts allows low-friction rotation of linkage bars, which makes force transmission smooth and efficient. Torsion springs are integrated to reduce the amount of actuation.

3.3.2 Tactile Sensing Components

The tactile sensing components consist of mirrors, acrylics, silicone pads, a Raspberry Pi camera and LED strips. The mirrors are made from 0.5 mm PEG flexible mirror sheets with a laser cutter, which can be easily attached to any flat or developable surfaces. The clear

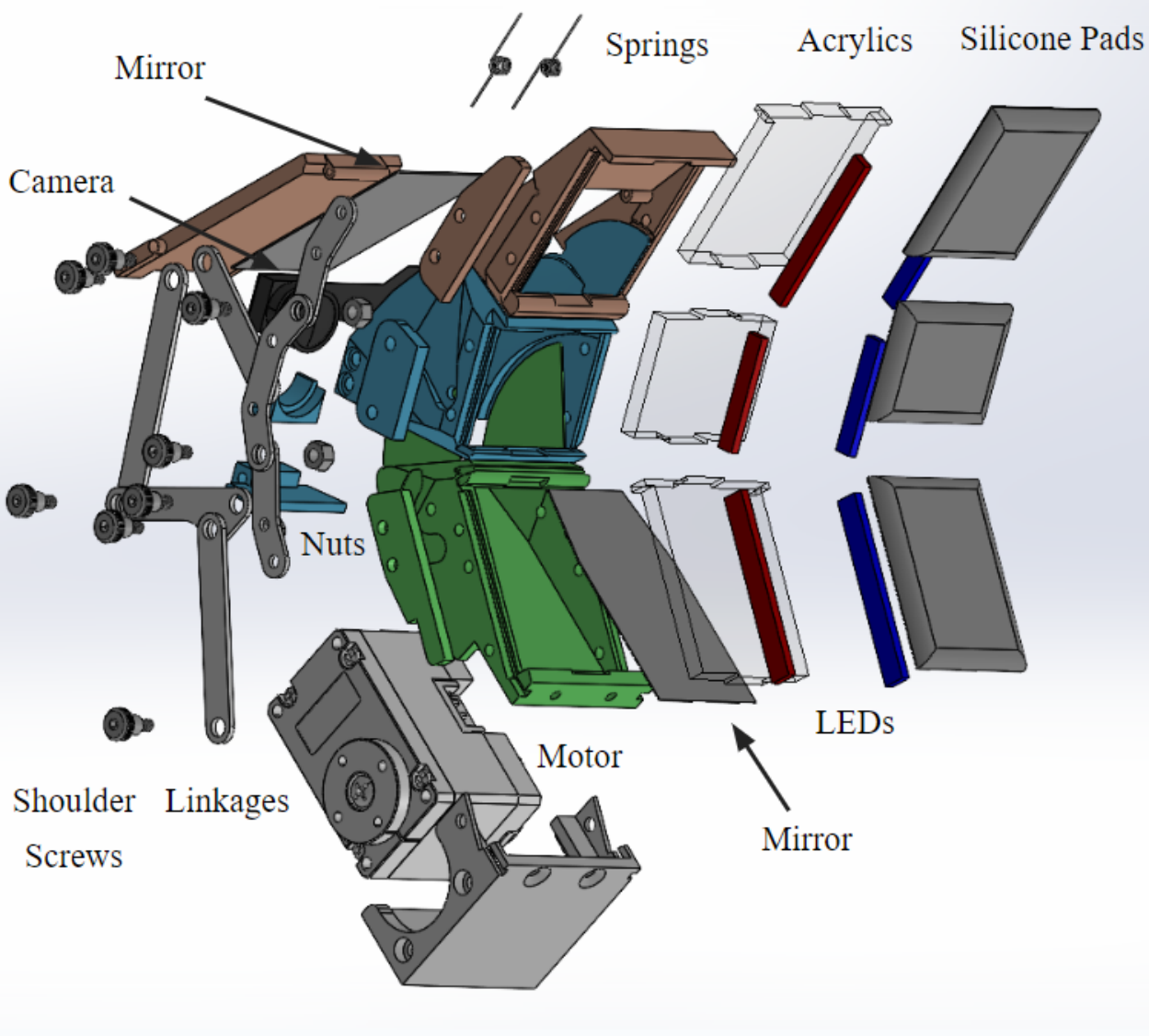

Figure 3.6: Exploded view of the proposed robotic finger.

silicone pads are coated with gray paint to provide Lambertian reflection. Another popular paint in Gelsight sensors is silver paint, which provides Semi-specular reflection. Lambertian paint is employed in this design, because Lambertian surfaces provide more accurate gradient information, which helps to improve the quality of 3d reconstruction. Semi-specular surfaces provide higher sensitivity but with less accurate image gradients [33]. We mix XP-565 Parts A and B Silicones Inc.) and a plasticizer (LC1550 Phenyl Trimethicone, Lotioncrafter) with a 1 to 15 to 3 parts ratio to make soft sensing pads. The Lambertian paint is made of 1 part silicone ink catalyst to 10 parts gray silicone ink base to 2.5 parts 4 μm aluminum cornflakes

to 30 parts NOVOCS Gloss (Raw Materials Inc., Schlenk, Smooth-on Inc), which is similar to the recipe used in our previous paper [4]. The piant was sprayed on the silicone pads to obtain an even distribution. Clear acrylic pieces were cut to support the soft silicone pads without blocking lights.

In order to integrate directional illumination with different colors, blue and red flexible COB LED strips (4mm COB LED strip light, OCONA) are attached to the sides of acrylic pieces, with color filters attached to prevent unwanted light reradiation. A Raspberry Pi Zero Spy camera with a high FOV of 160 degrees is used to achieve a large sensing range, and the video is streamed by mjpg streamer on the Raspberry Pi, and parse the mjpeg video stream from python on a computer. With a Raspberry Pi 4B board, 30 FPS can be achieved for 1440×1080 pixels. To get stable and well-blend color images, it is important to turn off the AWB (auto white balance), and tune fixed gains for awbgainR (red channel), awbgainB (blue channel), and EV (exposure compensation for RGB channels) [22].

Chapter 4

Tactile Sensing and Proprioception

With the integrated tactile sensor, the relative positions of the camera, the mirrors and the finger pads changes as the finger moves, which further leads to perspective changing in the raw image. Therefore, the raw image contains a mixed information of both tactile data and finger movement. This chapter elaborates on the image processing algorithm that unwarps tactile images and extracts proprioception information from the image. Unwarped tactile images can be used to generate difference images, which put more emphasis on changes in the tactile properties of a surface or object. Moreover, 3d reconstruction also prefers difference images. Proprioception for underactuated fingers could mitigate the problem of independent actuation and help the control system to regulate the finger's behavior by providing accurate finger postures.

4.1 Tactile Sensing

In this section, a workflow of extracting undistorted tactile images is introduced in detail. As Fig. 4.1 (b) presents, from top to bottom, the raw image records the mirror view and direct view of the distal contact pad, the direct view of the intermediate contact pad, and the mirror view and direct view of the proximal contact pad. The workflow in Fig. 4.1 (c) is utilized to detect all image views, pick an optimal view for each finger pad, and create

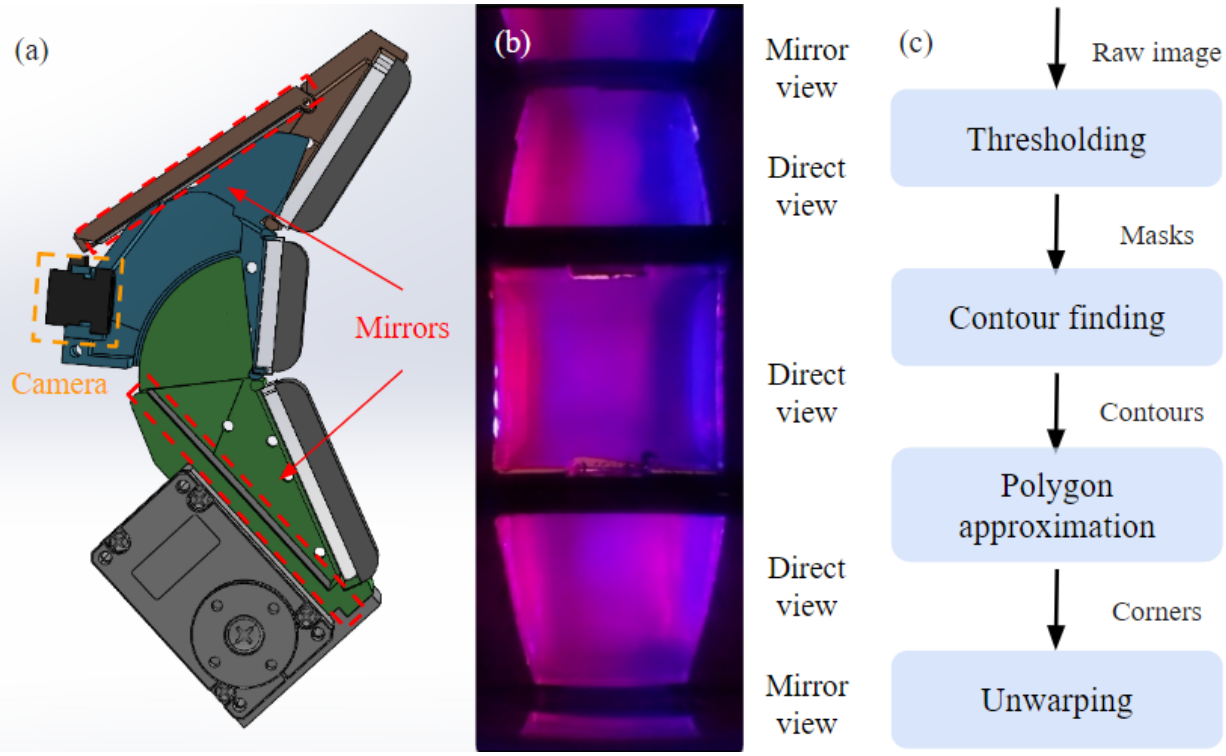

Figure 4.1: (a) Section view of the finger with camera and mirrors highlighted; (b) Raw image captured by the embedded camera; (c) Workflow of image processing algorithm to extract unwarped image.

unwarped tactile images.

4.1.1 Methods

As shown in Fig. 4.1 (c), tactile image processing has four main steps, generating image segmentation masks by thresholding, detecting tactile image contours, extracting feature corners of the contours with polygon approximation, and unwarping tactile images by constructing affine transformation. The whole processing is written in Python using the opencv-python library [34].

Fig. 4.2 shows the process of applying image thresholding. First, RGB image in Fig. 4.1 (b) is converted to grayscale image in Fig. 4.1 (a). Then, different thresholding methods can be applied to the single-channel grayscale image. Opencv provides three popular threshoding method, simple thresholding (global thresholding), adaptive thresholding, and

Otsu's thresholding. Global thresholding applies a specified and constant thresholding value to the whole image and works better when illumination is uniform, adaptive thresholding determines a variable threshold for a pixel based on a small region of its neighbor pixels and can overcome nonuniform lighting conditions, and Otsu's method automatically determines an optimal threshold that divides the image into two distinct regions for all pixels. Because environmental lights are obstructed, pixels belonging to tactile images are brighter, but the internal surfaces of phalanges still reflect some amount of lights. Thus, global thresholding method can segment good global masks with poor corner quality, as shown in Fig. 4.2 (b). Meanwhile, the rgb-to-grayscale conversion leads to nonuniform grayscale values, which introduce errors to adaptive thresholding, as shown in Fig. 4.2 (c). Finally, by combing gloabl thresholding and adaptive thresholding, global masks with accurate corners can be generated.

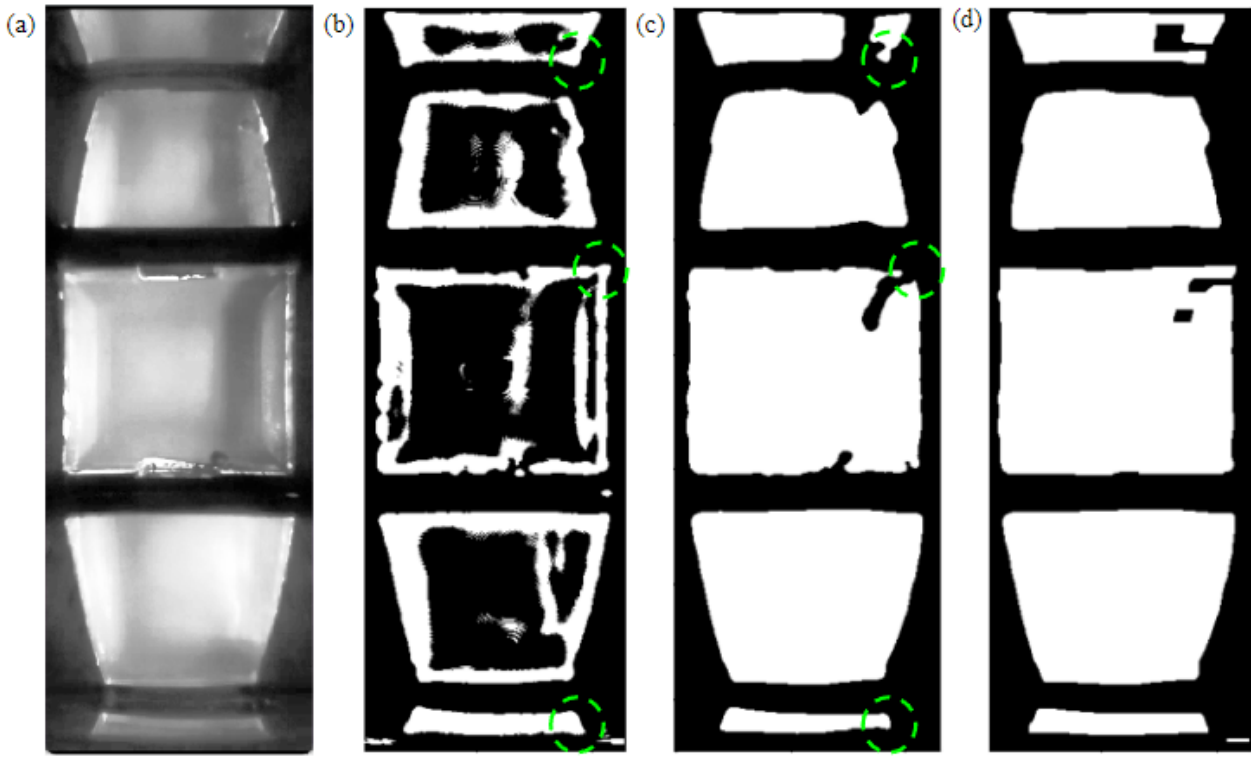

Figure 4.2: From left to right: gray scale image, adaptive thresholding image, global value thresholding image and combined thresholding image.

After thresholding, tactile image masks are denoised with opening and closing algorithms. Then, contours can be easily found with the $find_contours$ function in opencv. The contours highlighted by red lines in Fig 4.3 have noisy boundaries due to imperfections in fabrication. The contours are then smoothened by finding the convex hulls, which is denoted by blue lines in Fig. 4.3 (c). After that, convex hulls are fed to the polygon approximation algorithm in opencv, which adapts contours with polygons and outputs the feature corners highlighted by green dots in Fig. 4.3.

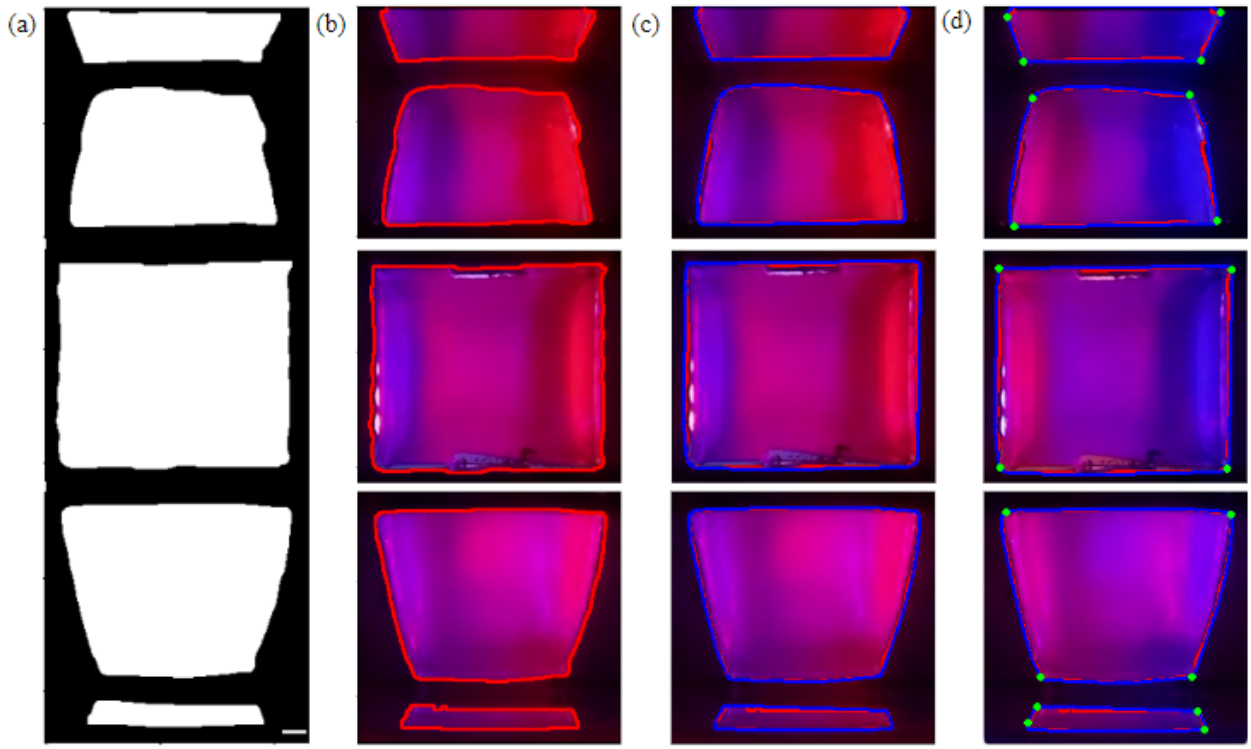

Figure 4.3: From left to right: denoised mask, contour finding (highlighted by red lines), convex hull (highlighted by blue lines) and polygon approximation (highlighted by green dots)

The elastomer pads have rectangular shapes, which warp into quadrilaterals in the captured image. After the above image processing, four corners of the quadrilaterals are detected, which can be used to form affine transformations from warped images to unwarped images. Fig. 4.4 shows the process of generating unwarping tactiles images. In most configurations, the camera captures both mirror view and direct view of the distal and proximal

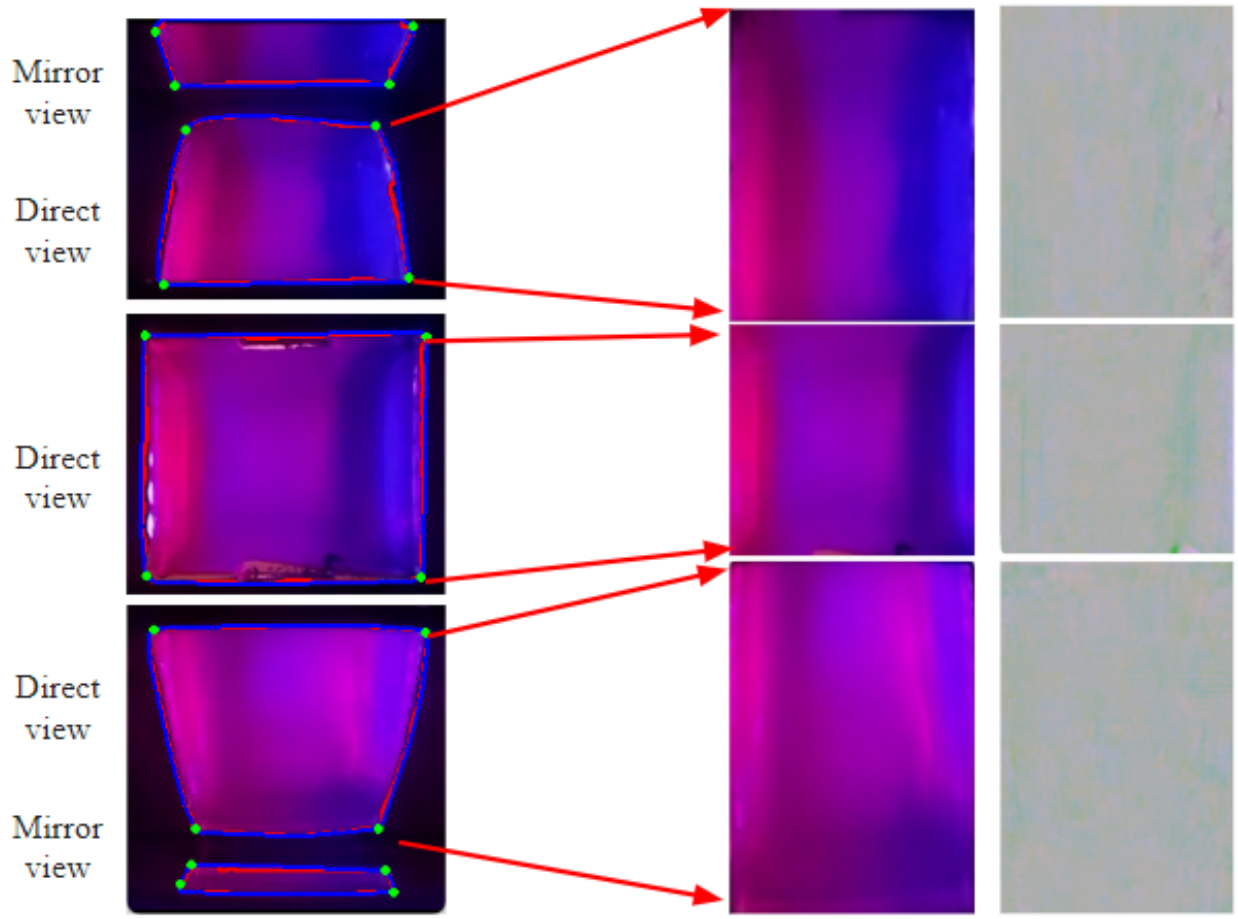

Figure 4.4: Unwarping tactile images with detected corner points with direct view or mirror view. From left to right: unwarped images and difference images.

contact pads. In this paper, the image view with a bigger area is chosen because it contains richer information. Difference images are computed by subtracting a reference unwarped image from a deformed unwarped image. Difference images emphasize more on the relative deformation and thus become a better representation of tactile information. As shown in Fig. 4.4, there are some artifacts in the difference images. The possible error sources are image distortion from a large field-of-view lens, computational errors in image processing and imperfections during fabrication.

4.1.2 Results

Fig. 4.5 shows the case when the robotic finger touched a lego piece. As the figure shows, only distal contact pad touched the lego piece, and imprints of lego extrusions can be seen in the corresponding tactile images, among which the difference image shows the best comparison. The intermediate tactile image shows some imprint pattern because the intermediate sensing pad touched the white box under the lego piece.

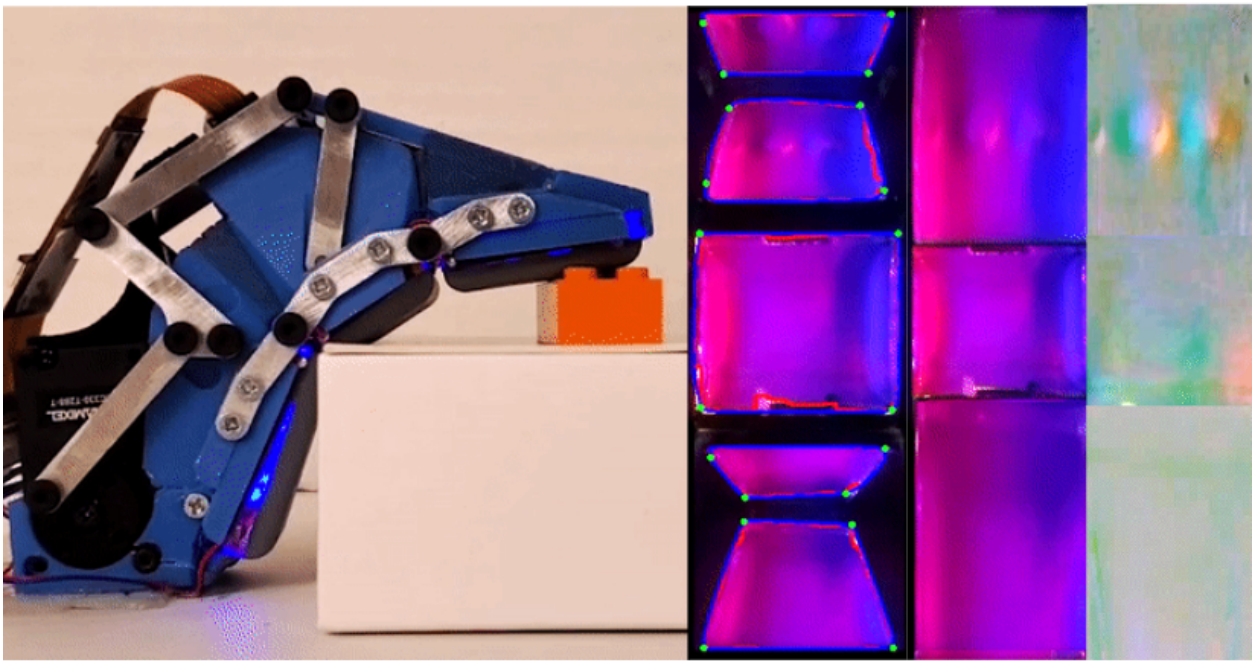

Figure 4.5: Robotic finger touches a lego piece. From left to right: experiment setup, raw images captured by the embedded camera, unwarped tactile images of three phalanges, and the corresponding difference images

To demonstrate the ability of continuous sensing, we used an array of calibration balls, a lego piece, a M2.5 heat insert, a plastic orange, and a golf ball to touch different phalanges of the robotic finger. The tactile images reflect that the illumination on different gel pads are not uniform. The tactile images of the distal and proximal phalanges are dimmer than those of the intermediate phalanx. Although the non-uniform illumination has less affect on difference images, unwarped raw images are still very useful in applications that uses machine learning, such as learning-based manipulation and property estimation. This problem can

be directly mitigated with light diffusers, and we will also explore ways to compensate non-uniform illumination in the future. Fig. 4.6 presents the tactile imprints of these touchings. The ability could provide detailed information of grasped objects, which might benefit in-hand object classification, in-hand pose estimation, and in-hand manipulation.

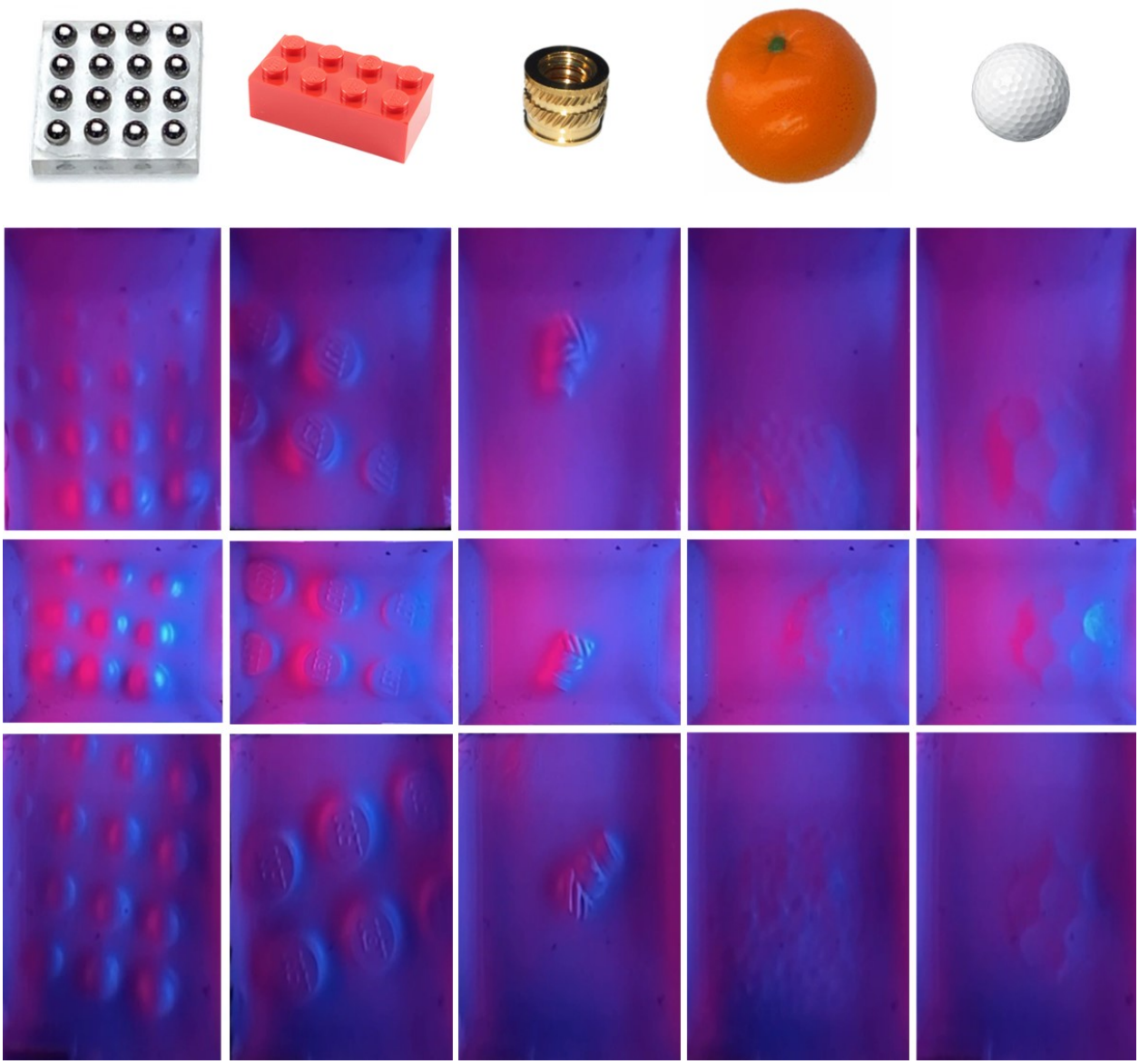

Figure 4.6: Tactile images of distal, intermediate, and proximal phalanges touching an array of calibration balls, a lego piece, a M2.5 heat insert, a plastic orange, and a golf ball. From top to bottom: pictures of testing objects, tactile images of distal, intermediate, and proximal phalanges

4.2 Proprioception

4.2.1 Methods

By combing optical reflection simulation in section 3.2 and corner detection of tactile sensing, a proprioception algorithm is established. In the raw image captured by the embedded camera, there are gaps between mirror views and direct views, which is the space between the two green lines in Fig. 4.7. The width of the image gap can be estimated in the reflection simulation. After that, a lookup table can be constructed from the optical simulation. After the corner detection in tactile image processing, the image gaps can be computed from raw images, which can be used to estimate joint angles via lookup table. Due to fabrication errors, the algorithm has to be calibrated with at least five frames of labelled images, with which a reasonable accuracy can be obtained.

4.2.2 Results

Table 4.1 shows the absolute proprioception errors of 30 random frames. The absolute errors of proximal interphalangeal joint and distal interphalangeal joint are 2.3 $\pm$ 1.6 deg and 2.5 $\pm$ 2.0 deg.

Table 4.1: Absolute error in proprioception

	absolute errors
proximal interphalangeal joint	2.3 $\pm$ 1.6 deg
Distal interphalangeal joint	2.5 $\pm$ 2.0 deg

The error could come from both ground truth and proprioceptive measurements. First, manual measurement is not ideal and hard to evaluate the error. Moreover, it greatly limits the number of data points we can get because it is time-consuming and low-efficient. Our future work includes obtaining ground truth from mature vision systems, such as the Optitrack

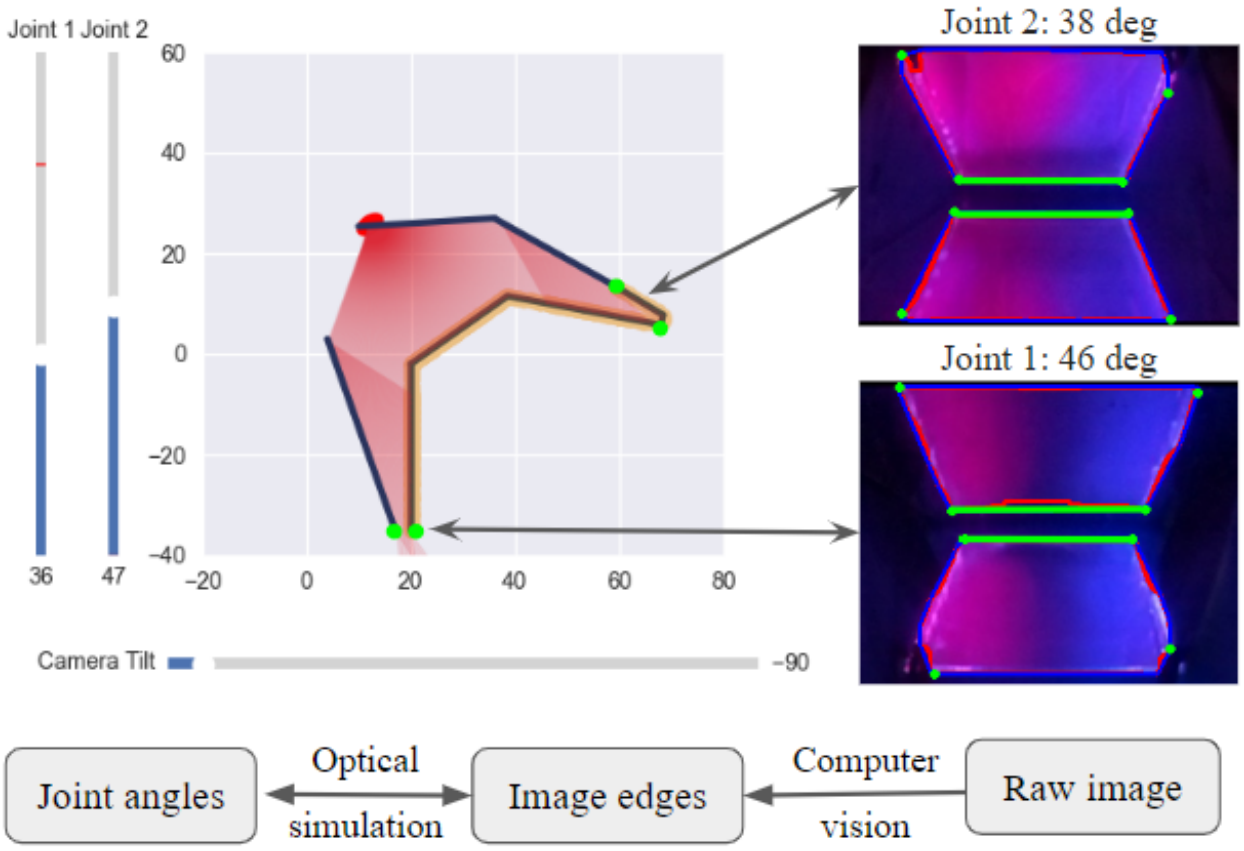

Figure 4.7: Proprioception algorithm. Joint 1 is proximal interphalangeal joint, and Joint 2 is distal interphalangeal joint.

system and April Tag. Secondly, the error sources in proprioceptive measurements include fabrication imperfections, position error of the camrea and gel pads, and computational errors in image processing algorithms.

The ground truth was obtained manually in Fig. 4.8, and detected joint angles are shown in the linkage simulator.

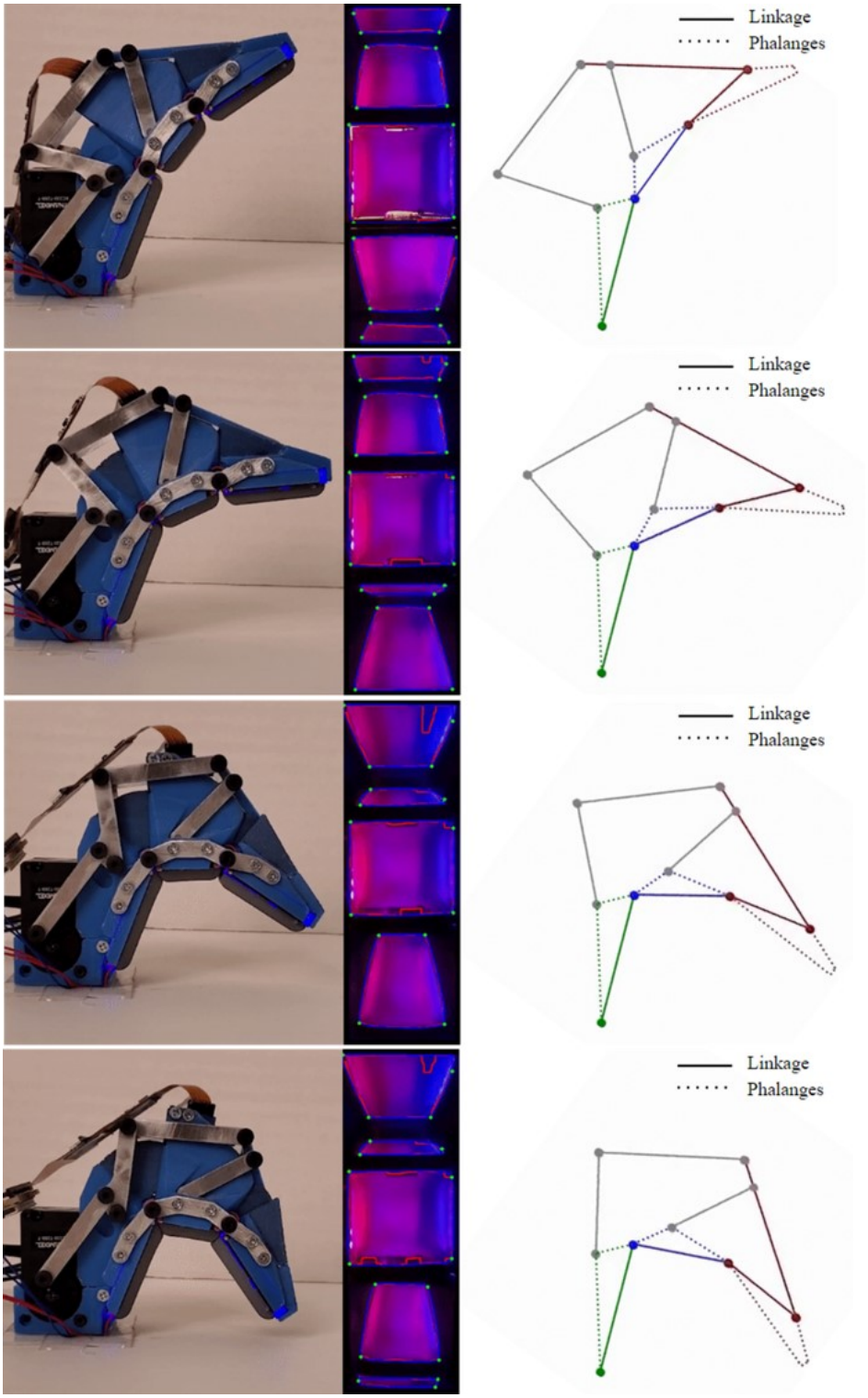

Figure 4.8: Left: ground truth configuration of the finger and the corresponding tactile image. Right: estimated configuration of the proprioception algorithm shown with the linkage simulator

Chapter 5

Conclusion and Future work

In summary, this thesis presents a comprehensive exploration of the design and integration of an underactuated linkage finger enhanced with vision-based tactile sensing. The research journey led to the development of a compact and adaptable finger mechanism that combines underactuation and tactile perception, offering robustness and versatility in grasping tasks. By strategically incorporating a low-cost, simple vision-based tactile sensor, namely GelSight, this work addresses the challenge of control complexity often associated with underactuated fingers.

The iterative design process encompassed three pivotal stages, each refining the finger's structure and functionality. The initial iteration introduced sliding joints, succeeded by the incorporation of more compact and robust linkage mechanisms in the second iteration. A novel planar linkage simulator was employed to optimize motion trajectories and prevent collisions, thereby enhancing the finger's overall performance. The final design evolution embraced the integration of a third finger segment with underactuation, effectively minimizing motor requirements. Crucially, each finger segment houses a silicone gel pad, with tactile information captured via mirrors and observed by a single camera strategically positioned within the second finger segment. The arrangement of mirrors, alongside the innovative use of linkage transmission and underactuation, culminates in a mechanism that is both

efficient and streamlined. This synergy not only reduces the necessity for multiple cameras and motors but also empowers the finger to perceive both contact information and its own configuration.

The incorporation of vision-based tactile sensors holds immense promise in expanding the horizons of underactuated fingers. This integration not only enables the execution of tasks under challenging conditions, such as sub-optimal lighting or occluded objects, but also opens avenues for object identification akin to human-like proprioception. Through rigorous testing and simulation, the integration of vision-based sensors has proven instrumental in equipping the underactuated finger with high-resolution imagery and proprioceptive insights, effectively bridging the gap between tactile perception and efficient manipulation.

This thesis encapsulates a pioneering exploration into the symbiotic fusion of underactuation and tactile sensing, yielding a cutting-edge underactuated linkage finger. The outcome showcases a novel approach to designing compact, adaptable, and robust mechanisms for proficient grasping tasks. By harnessing the power of vision-based tactile sensors, the research not only overcomes control challenges but also redefines the capabilities of underactuated fingers. This innovative design can potentially enhance the performance of underactuated fingers and hands in dexterous tasks and thus expand their application in industries such as manufacturing and assembly, daily tasks such as cooking and serving, and healthcare such as rehabilitation and prosthesis.

This work is still with a few limitations. First, robotic finger can not be widely used without a proper hand design. Although the finger shows adaption to various objects, a well-designed hand will achieve much better performance in grasping and manipulation tasks. One important work to be finished in the future is to design palms and arrange fingers so that the hand will be able to make good use of the benefits of underactuation and vision-based tactile sensing. Second, the tactile images from different sensing pads show some distortion and non-uniform illumination. In the future, the images will be undistorted with calibrated camera model, and we will explore solutions to obtain better illunimation with both hardware

and software. Third, the error analysis for proprioception need to be improved. Currently, the ground truth is manually measured, which greatly limits the number of samples that can be used. In order to improve the quality of proprioception, estimation error has to be analyzed at different configurations, which can not be done with tens of data points. In future work, we will use April tag or optitrack system to acquire large amount of labelled data, and a more thorough error analysis will be implemented. Finally, the gripping force is not evaluated in this work, which will allow us to optimize the force performance of the linkage. Other than evaluating with experiments, mathematical models of underactuated linkages can be established. We will characterize the gripping force of the finger or the hand we will design in future both mathematically and experimentally.

References

[1] C.-H. Xiong, W.-R. Chen, B.-Y. Sun, M.-J. Liu, S.-G. Yue, and W.-B. Chen, "Design and implementation of an anthropomorphic hand for replicating human grasping functions," *IEEE Transactions on Robotics*, vol. 32, no. 3, pp. 652–671, 2016.

[2] J. Martin and M. Grossard, "Design of a fully modular and backdrivable dexterous hand," *The International Journal of Robotics Research*, vol. 33, no. 5, pp. 783–798, 2014.

[3] U. Kim, D. Jung, H. Jeong, J. Park, H.-M. Jung, J. Cheong, H. R. Choi, H. Do, and C. Park, "Integrated linkage-driven dexterous anthropomorphic robotic hand," *Nature communications*, vol. 12, no. 1, p. 7177, 2021.

[4] S. Q. Liu, Y. Ma, and E. H. Adelson, "Gelsight baby fin ray: A compact, compliant, flexible finger with high-resolution tactile sensing," in *2023 IEEE International Conference on Soft Robotics (RoboSoft)*, IEEE, 2023, pp. 1–8.

[5] S. Q. Liu and E. H. Adelson, "Gelsight fin ray: Incorporating tactile sensing into a soft compliant robotic gripper," in *2022 IEEE 5th International Conference on Soft Robotics (RoboSoft)*, IEEE, 2022, pp. 925–931.

[6] H. Wang, H. Xu, F. J. Abu-Dakka, V. Kyrki, C. Yang, X. Li, and S. Chen, "A bidirectional soft biomimetic hand driven by water hydraulic for dexterous underwater grasping," *IEEE Robotics and Automation Letters*, vol. 7, no. 2, pp. 2186–2193, 2022.

[7] M. Maggi, G. Mantriota, and G. Reina, "Introducing polypus: A novel adaptive vacuum gripper," *Mechanism and Machine Theory*, vol. 167, p. 104 483, 2022.

[8] S. Puhlmann, J. Harris, and O. Brock, "Rbo hand 3: A platform for soft dexterous manipulation," *IEEE Transactions on Robotics*, vol. 38, no. 6, pp. 3434–3449, 2022.

[9] *Shadow hand website*, https://www.shadowrobot.com/dexterous-hand-series/, Accessed: 2023-08-01.

[10] *Allegro hand wiki*, http://wiki.wonikrobotics.com/AllegroHandWiki/, Accessed: 2023-08-01.

[11] F. Hundhausen, J. Starke, and T. Asfour, "A soft humanoid hand with in-finger visual perception," in *2020 IEEE/RSJ International Conference on Intelligent Robots and Systems (IROS)*, IEEE, 2020, pp. 8722–8728.

[12] C. Gosselin, F. Pelletier, and T. Laliberte, "An anthropomorphic underactuated robotic hand with 15 dofs and a single actuator," in *2008 IEEE International Conference on Robotics and Automation*, IEEE, 2008, pp. 749–754.

[13] M. G. Catalano, G. Grioli, E. Farnioli, A. Serio, C. Piazza, and A. Bicchi, "Adaptive synergies for the design and control of the pisa/iit softhand," *The International Journal of Robotics Research*, vol. 33, no. 5, pp. 768–782, 2014.

[14] G. Jia, G. Chen, and M. Xie, "Design of a novel compact dexterous hand for teleoperation," in *Proceedings 2001 IEEE International Symposium on Computational Intelligence in Robotics and Automation (Cat. No. 01EX515)*, IEEE, 2001, pp. 5–10.

[15] C. Della Santina, G. Grioli, M. Catalano, A. Brando, and A. Bicchi, "Dexterity augmentation on a synergistic hand: The pisa/iit softhand+," in *2015 IEEE-RAS 15th International Conference on Humanoid Robots (Humanoids)*, IEEE, 2015, pp. 497–503.

[16] R. Wang, S. Wang, S. Du, E. Xiao, W. Yuan, and C. Feng, "Real-time soft body 3d proprioception via deep vision-based sensing," *IEEE Robotics and Automation Letters*, vol. 5, no. 2, pp. 3382–3389, 2020.

[17] A. J. Spiers, M. V. Liarokapis, B. Calli, and A. M. Dollar, "Single-grasp object classification and feature extraction with simple robot hands and tactile sensors," *IEEE transactions on haptics*, vol. 9, no. 2, pp. 207–220, 2016.

[18] Z. Lu, H. Guo, W. Zhang, and H. Yu, "Gtac-gripper: A reconfigurable under-actuated four-fingered robotic gripper with tactile sensing," *IEEE Robotics and Automation Letters*, vol. 7, no. 3, pp. 7232–7239, 2022.

[19] V. Prado da Fonseca, T. E. Alves de Oliveira, and E. M. Petriu, "Estimating the orientation of objects from tactile sensing data using machine learning methods and visual frames of reference," *Sensors*, vol. 19, no. 10, p. 2285, 2019.

[20] M. H. Tippur and E. H. Adelson, "Gelsight360: An omnidirectional camera-based tactile sensor for dexterous robotic manipulation," in *2023 IEEE International Conference on Soft Robotics (RoboSoft)*, IEEE, 2023, pp. 1–8.

[21] M. Lambeta, P.-W. Chou, S. Tian, B. Yang, B. Maloon, V. R. Most, D. Stroud, R. Santos, A. Byagowi, G. Kammerer, *et al.*, "Digit: A novel design for a low-cost compact high-resolution tactile sensor with application to in-hand manipulation," *IEEE Robotics and Automation Letters*, vol. 5, no. 3, pp. 3838–3845, 2020.

[22] S. Wang, Y. She, B. Romero, and E. Adelson, "Gelsight wedge: Measuring high-resolution 3d contact geometry with a compact robot finger," in *2021 IEEE International Conference on Robotics and Automation (ICRA)*, IEEE, 2021, pp. 6468–6475.

[23] H. Sun, K. J. Kuchenbecker, and G. Martius, "A soft thumb-sized vision-based sensor with accurate all-round force perception," *Nature Machine Intelligence*, vol. 4, no. 2, pp. 135–145, 2022.

[24] W. Yuan, S. Dong, and E. H. Adelson, "Gelsight: High-resolution robot tactile sensors for estimating geometry and force," *Sensors*, vol. 17, no. 12, p. 2762, 2017.

[25] I. H. Taylor, S. Dong, and A. Rodriguez, "Gelslim 3.0: High-resolution measurement of shape, force and slip in a compact tactile-sensing finger," in *2022 International Conference on Robotics and Automation (ICRA)*, IEEE, 2022, pp. 10 781–10 787.

[26] W. K. Do and M. Kennedy, "Densetact: Optical tactile sensor for dense shape reconstruction," in *2022 International Conference on Robotics and Automation (ICRA)*, IEEE, 2022, pp. 6188–6194.

[27] A. Yamaguchi and C. G. Atkeson, "Combining finger vision and optical tactile sensing: Reducing and handling errors while cutting vegetables," in *2016 IEEE-RAS 16th International Conference on Humanoid Robots (Humanoids)*, IEEE, 2016, pp. 1045–1051.

[28] A. Padmanabha, F. Ebert, S. Tian, R. Calandra, C. Finn, and S. Levine, "Omnitact: A multi-directional high-resolution touch sensor," in *2020 IEEE International Conference on Robotics and Automation (ICRA)*, IEEE, 2020, pp. 618–624.

[29] A. Wilson, S. Wang, B. Romero, and E. Adelson, "Design of a fully actuated robotic hand with multiple gelsight tactile sensors," *arXiv preprint arXiv:2002.02474*, 2020.

[30] Z. Li, F. Miao, Z. Yang, and H. Wang, "An anthropometric study for the anthropomorphic design of tomato-harvesting robots," *Computers and Electronics in Agriculture*, vol. 163, p. 104 881, 2019.

[31] *Mechanism python library*, https://github.com/gabemorris12/mechanism, Accessed: 2023-08-05.

[32] J. Angeles, *Rational kinematics*. Springer Science & Business Media, 2013, vol. 34.

[33] S. Dong, W. Yuan, and E. H. Adelson, "Improved gelsight tactile sensor for measuring geometry and slip," in *2017 IEEE/RSJ International Conference on Intelligent Robots and Systems (IROS)*, IEEE, 2017, pp. 137–144.

[34] G. Bradski, "The OpenCV Library," *Dr. Dobb's Journal of Software Tools*, 2000.